This is the peer reviewed author accepted manuscript (post print) version of a published work that appeared in final form in:

Stead, Sebastian O, Kireta, Svjetlana, McInnes, Steve JP, Kette, Francis D, Sivanathan, Kisha N, Kim, Juewan, Cueto-Diaz, Eduardo J, Cunin, Frederique, Durand, Jean Olivier, Drogemuller, Christopher J, Carroll, Robert P 2018 'Murine and non-human primate dendritic cell targeting nanoparticles for in vivo generation of regulatory t-cells', ACS Nano, vol. 12, no. 7, pp. 6637-6647

This un-copyedited output may not exactly replicate the final published authoritative version for which the publisher owns copyright. It is not the copy of record. This output may be used for non-commercial purposes.

The final definitive published version (version of record) is available at:
https://doi.org/10.1021/acsnano.8b01625

Persistent link to the Adelaide University Research Outputs Repository:
http://hdl.handle.net/2440/114096

General Rights
Copyright and moral rights for the publications made accessible in the Adelaide Research Outputs Repository are retained by the authors and/or other copyright owners and it is a condition of accessing publications that users recognize and abide by the legal requirements associated with these rights.

- Users may download and print one copy for the purpose of private study or research.
- You may not further distribute the material or use it for any profit-making activity or commercial gain
- You may freely distribute the persistent link identifying the publication in the UniSA Research Outputs Repository

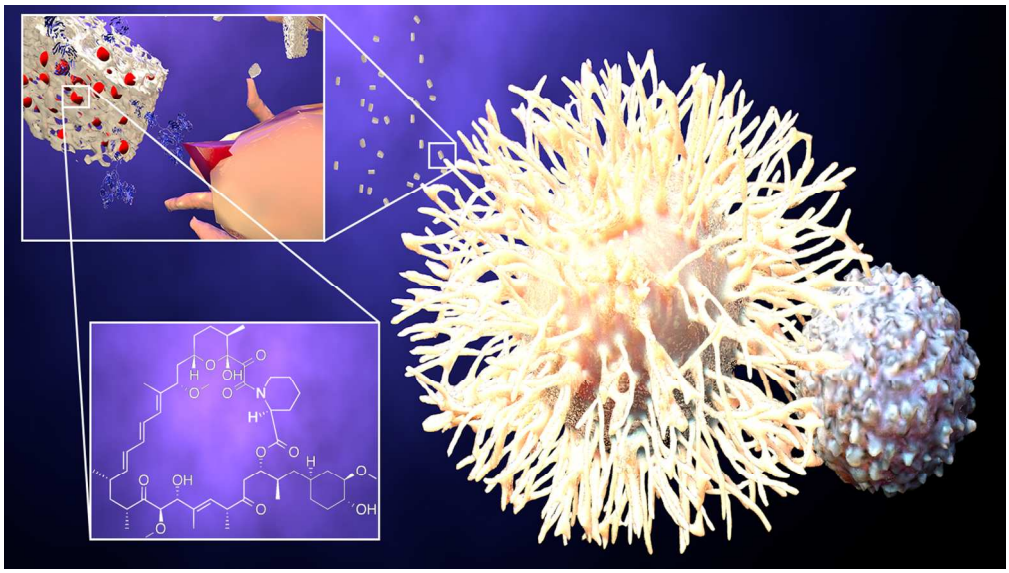
If you believe that this document breaches copyright, please contact us and provide details. We will remove access to the work immediately and investigate your claim.

This document is confidential and is proprietary to the American Chemical Society and its authors. Do not copy or disclose without written permission. If you have received this item in error, notify the sender and delete all copies.

Murine and Non-Human Primate Dendritic Cells Targeting Nanoparticles for In Vivo Generation of Regulatory T-cells

Journal:	*ACS Nano*
Manuscript ID	nn-2018-01625g
Manuscript Type:	Article
Date Submitted by the Author:	01-Mar-2018
Complete List of Authors:	Stead, Sebastian; University of Adelaide Faculty of Medicine Kireta, Svjetlana; Royal Adelaide Hospital McInnes, Steven; University of South Australia, Future Industries Institute Kette, Francis; University of Adelaide Faculty of Medicine Sivanathan, Kisha; University of Adelaide Faculty of Medicine Kim, Juewan; University of Adelaide Faculty of Medicine Cueto-Diaz, Eduardo; Institut Charles Gerhardt Montpellier, UMR 5253 CNRS-ENSCM-UM2-UM1 Matériaux Avancés pour la Catalyse et la Santé, Ecole Nationale Supérieure de Chimie Cunin, Frederique; Institut Charles Gerhardt Montpellier, UMR 5253 CNRS-ENSCM-UM2-UM1 Matériaux Avancés pour la Catalyse et la Santé, Ecole Nationale Supérieure de Chimie Durand, Jean-Olivier; Université Montpellier 2, UMR 5253 case 1701 Drogemuller, Christopher; University of Adelaide Faculty of Medicine; Royal Adelaide Hospital Carroll, Robert; University of Adelaide Faculty of Medicine; Royal Adelaide Hospital Voelcker, Nicolas; Monash Institute of Pharmaceutical Sciences, D4 Coates, P. Toby; University of Adelaide Faculty of Medicine; Royal Adelaide Hospital

SCHOLARONE™
Manuscripts



Cartoon rendering showing antibody coated porous silicon nanoparticles loaded with immunosuppressant, rapamycin, binding to a dendritic cell interacting with a T-lymphocyte.

508x286mm (72 x 72 DPI)

Title: Murine and Non-Human Primate Dendritic Cells Targeting Nanoparticles for In Vivo Generation of Regulatory T-cells

Authors: Sebastian O. Stead[1], Svjetlana Kireta[2], Steven J.P. McInnes[3], Francis D. Kette[1], Kisha N. Sivanathan[1], Juewan Kim[1], Eduardo J. Cueto-Diaz[4], Frédérique Cunin[4], Jean-Olivier Durand[4], Christopher J. Drogemuller[1,2], Robert P. Carroll[1,2], Nicolas H. Voelcker*[5,6,7,8], Patrick T. Coates*[1,2]

Affiliations:

[1]*University of Adelaide, Department of Medicine, Adelaide, Australia.*

[2]*Central Northern Adelaide Renal and Transplantation Service (CNARTS), The Royal Adelaide Hospital, Australia.*

[3]*Future Industries Institute, University of South Australia, Adelaide, Australia. 4Institut Charles Gerhardt Montpellier, case 1701, UMR 5253 CNRS -ENSCM-UM, 34095 Montpellier, cedex 5, France.*

[5]*Drug Delivery, Disposition and Dynamics, Monash Institute of Pharmaceutical Sciences, Monash University, 381 Royal Parade, Parkville, Victoria, Australia .*

[6]*Commonwealth Scientific and Industrial Research Organisation (CSIRO), Clayton, VIC, Australia.*

[7]*Melbourne Centre for Nanofabrication, Victorian Node of the Australian National Fabrication Facility, Clayton, VIC, Australia.*

[8]*Monash Institute of Medical Engineering, Monash University, Clayton, Victoria, Australia*

*co-senior authors.

‡ Corresponding authors. P.T. Coates: University of Adelaide, The Royal Adelaide Hospital Campus, Port Road, Adelaide 5000, Australia. Phone: (+618) 8222 0934. E-mail: toby.coates@sa.gov.au

N.H. Voelcker: Drug Delivery, Disposition and Dynamics, Monash Institute of Pharmaceutical Sciences, Monash University, 381 Royal Parade, Parkville VIC 3052, Australia. Phone: (+613) 9903 9230. E-mail: nicolas.voelcker@monash.edu

Abstract

Porous silicon nanoparticles (pSiNP), modified to target dendritic cells (DC), provide a novel strategy for the delivery of immunosuppressive drugs. Here, we aimed to develop a DC-targeting pSiNP displaying c-type lectin; Dendritic Cell-Specific Intercellular adhesion molecule-3-Grabbing Non-integrin (DC-SIGN) and CD11c monoclonal antibodies. The *in vivo* tracking of these fluorescent DC-targeting nanoparticles was assessed in both C57BL/6 mice and common marmosets (Callithrix jacchus) by i.v. injection (20 mg/kg). Rapamycin and ovalbumin $(OVA)_{323-339}$ peptide loaded pSiNP were employed to evaluate their ability to generate murine $CD4^+CD25^+FoxP3^+$ regulatory T-cells *in vivo* within OVA sensitised mice. *In vivo,* pSiNP migrated to the liver, kidneys, lungs and spleen in both mice and marmosets. Flow cytometry confirmed pSiNP uptake by splenic and peripheral blood DC when functionalised with targeting antibodies. C57BL/6 OVA sensitised mice injected with CD11c-pSiNP loaded with rapamycin + $OVA_{323-339}$ produced a 5-fold higher number of splenic regulatory T-cells compared to control mice, at 40 days post pSiNP injection. These results demonstrate the importance of pSiNP functionalisation with targeting antibodies to enhance cellular uptake and affords on opportunity for the *in vivo* generation of splenic regulatory T-cells.

Keywords: Rapamycin, Tregs, Nanoparticles, porous silicon, Nanomedicine, tolerance, DC-SIGN

Long-term transplant survival is significantly hindered by chronic graft rejection, however increased susceptibility to infection and malignancies are major complications of prolonged immunosuppression.[1] Ideally, patients could maintain a functional organ devoid of

immunosuppressive medication, by promoting donor-specific immune hypo-responsiveness or "immune tolerance", significantly reducing the risk of developing cancer and infection. This has been termed the 'holy grail' of transplantation since first proposed in the 1950's.[2]

Dendritic cells (DC) within the immune system are responsible for processing and presenting foreign peptides, inducing an immune response towards an allogeneic transplant. DC are the most potent of the antigen presenting cells (APC), capable both of immunostimulation and immunosuppression and drive antigen specific tolerance by promoting regulatory T-cell (Treg) production.[3, 4] One promising approach is the induction of tolerance to allogeneic grafts via targeting DC with drug loaded nanoparticles designed to dampen immune responsiveness and generate 'tolerogenic DC' (tol-DC). The use of tol-DC in transplantation, as an immune therapy has developed significant traction in recent years, with several clinical trials investigating the benefits of *in vivo* DC therapy.[5, 6]

Rapamycin is a commonly used immunosuppressive medication that promotes formation of tol-DC.[7] Preconditioning DC with rapamycin induces a maturation resistant phenotype, characterised by decreased co-stimulatory and maturation markers expression,[8-10] which can induce T-cell anergy and promote Treg generation.[11] DC also express specific surface molecules including the c-type lectin, Dendritic Cell-Specific Intercellular adhesion molecule-3-Grabbing Non-integrin (DC-SIGN; CD209). Coupling DC-SIGN monoclonal antibodies to porous silicon drug-loaded nanoparticles creates a novel means to specifically target DC *in vivo*. Utilising targeting, drug-loaded nano-carriers that deliver therapeutics specifically to these key immune cells, has the potential to reduce off-targeted drug effects. Here, we studied the uptake of DC-targeting porous silicon nanoparticles (pSiNP), functionalised with antibodies to murine CD11c and human/non-human primate (NHP) DC-SIGN *in vivo*. Rapamycin loaded pSiNP were also assessed in their

ability to generate Treg *in vivo* in an ovalbumin (OVA) sensitised murine model. We utilised both a murine and NHP model to investigate the hypothesis that pSiNP functionalisation with DC-targeting antibodies would permit a higher level of cell targeting *in vivo* compared to their non-targeting counterparts.

Results

Murine DC targeting with CD11c-pSiNP

Murine CD11c has been used extensively to categorise myeloid lineage negative, MHC class II (MHC II)$^{+}$CD4^{+}CD8α^{-} and MHC II^{+}CD4^{-}CD8α^{+} DC subsets.[15] The highly unique expression of CD11c on myeloid DC subsets serves as a prime target for tracking within a murine model. Intravenous administration of isotype and CD11c-pSiNP accumulated within the kidneys within an hour. Whole body fluorescence dissipate in a time dependent manner (Figure 1A). However, quantification of organ fluorescence (Figure 1B-C) as radiant efficiencies (RE), the fluorescence emission radiance per incident excitation irradiance, showed both isotype and CD11c-pSiNP accumulation was time-dependant. Isotype-pSiNP mice showed a maximum pSiNP accumulation in the liver ($1.2x10^8$ RE), spleen ($2.2x10^7$ RE) and kidneys ($4.2x10^8$ RE) at 6 h and lungs ($2.1x10^7$ RE) at 12 h (Figure S1) with no significant heart uptake. Kidney fluorescence was 14-fold higher than the saline control at 6 and 24 h (Figure S1 & 1). CD11c-pSiNP mice had significantly higher pSiNP accumulation in the liver, lungs, heart, spleen and kidneys compared to both the saline and isotype-pSiNP control mice. Maximum fluorescence was seen in the liver ($2.3x10^8$ RE) and spleen ($1.2x10^8$ RE) at 24 h (Figure 1), and the lungs ($4.3x10^7$ RE), kidneys ($1.2x10^9$ RE) and heart ($1.6x10^7$ RE) at 12 h (Figure S1). CD11c-pSiNP accumulated 10-fold higher then isotype-pSiNP

in the spleen at 6 and 24 h, (Figure 1). CD11c-pSiNP mice splenic fluorescence decreased by approximately 60% from 6 to 12 h, accompanied by increased presence in the heart and kidneys at 12 h (Figure S1).

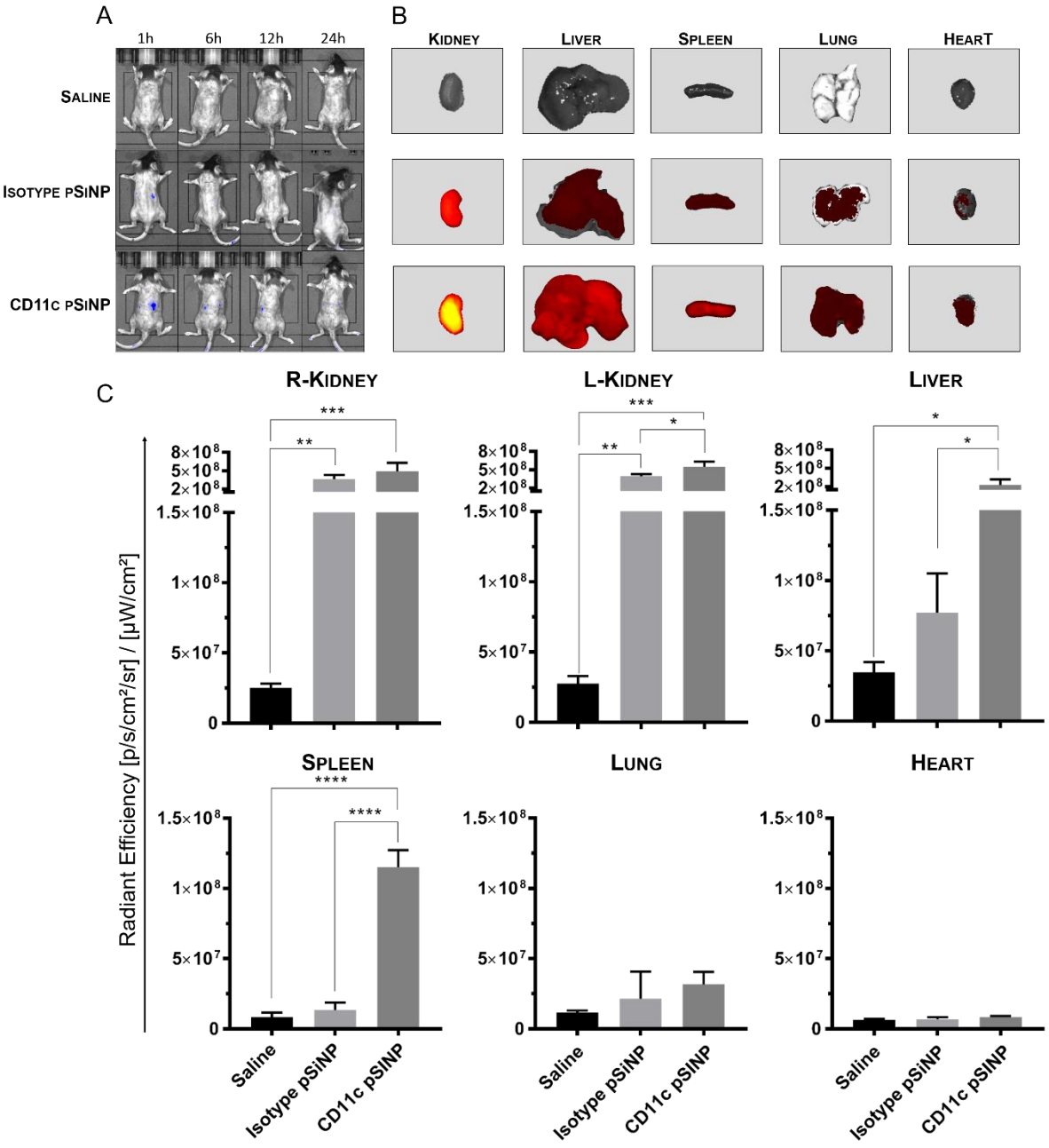


Figure 1. CD11c pSiNP track predominately to the kidneys, followed by the liver, spleen, lungs and heart. (A) Topographical distribution of fluorescent pSiNP over 1, 6, 12 and 24 h indicated by blue colour. High level of accumulation seen in the kidneys at 1 h which dissipated at 24 h. (B) Individual organs taken from the mice at 24 h post injection (i.v.) with fluorescent pSiNP. Heat map (red to yellow) indicates

presence of pSiNP. (C) Quantification of total fluorescence as radiant efficiencies of each of the organs at 24 h. Mice injected with CD11c pSiNP had an approximately 10-fold higher levels in the spleen compared to isotype pSiNP. CD11c pSiNP tracked significantly more to the kidneys and lungs of the mice compared to isotype pSiNP. Insignificant presence of pSiNP was seen within the lungs and heart. (Data is represented as mean ± SD, n = 3 per group, significance determined by one-way ANOVA, * $p < 0.05$, ** $p < 0.01$, *** $p < 0.001$, **** $p < 0.0001$).

Splenic MHC $II^+CD4^+CD8\alpha^-$ and MHC $II^+CD4^-CD8\alpha^+$ DC had a 9-fold and 31-fold higher fluorescence for CD11c-pSiNP respectively, compared to isotype-pSiNP (Figure 2). MHC $II^+CD11b^-CD11c^+$ splenic DC showed positivity for CD11c-pSiNP and no detectable levels of isotype-pSiNP (Figure 2). Splenic MHC $II^+CD11b^+CD11c^-$ macrophages[16] accumulated CD11c-pSiNP 4-fold higher than isotype-pSiNP after 24 h (Figure 2). CD11c-pSiNP were preferentially taken up by the MHC $II^+CD11c^+CD11b^-$ population within the peripheral blood, at 12 and 24 h, with no detectable uptake of isotype-pSiNP (Figure S2 and 2 respectively). Blood macrophages were positive for isotype-pSiNP at 1, 12 and 24 h, however, blood DC and macrophage populations indicated no significance uptake between isotype or CD11c-pSiNP (Figure S2 and 2).

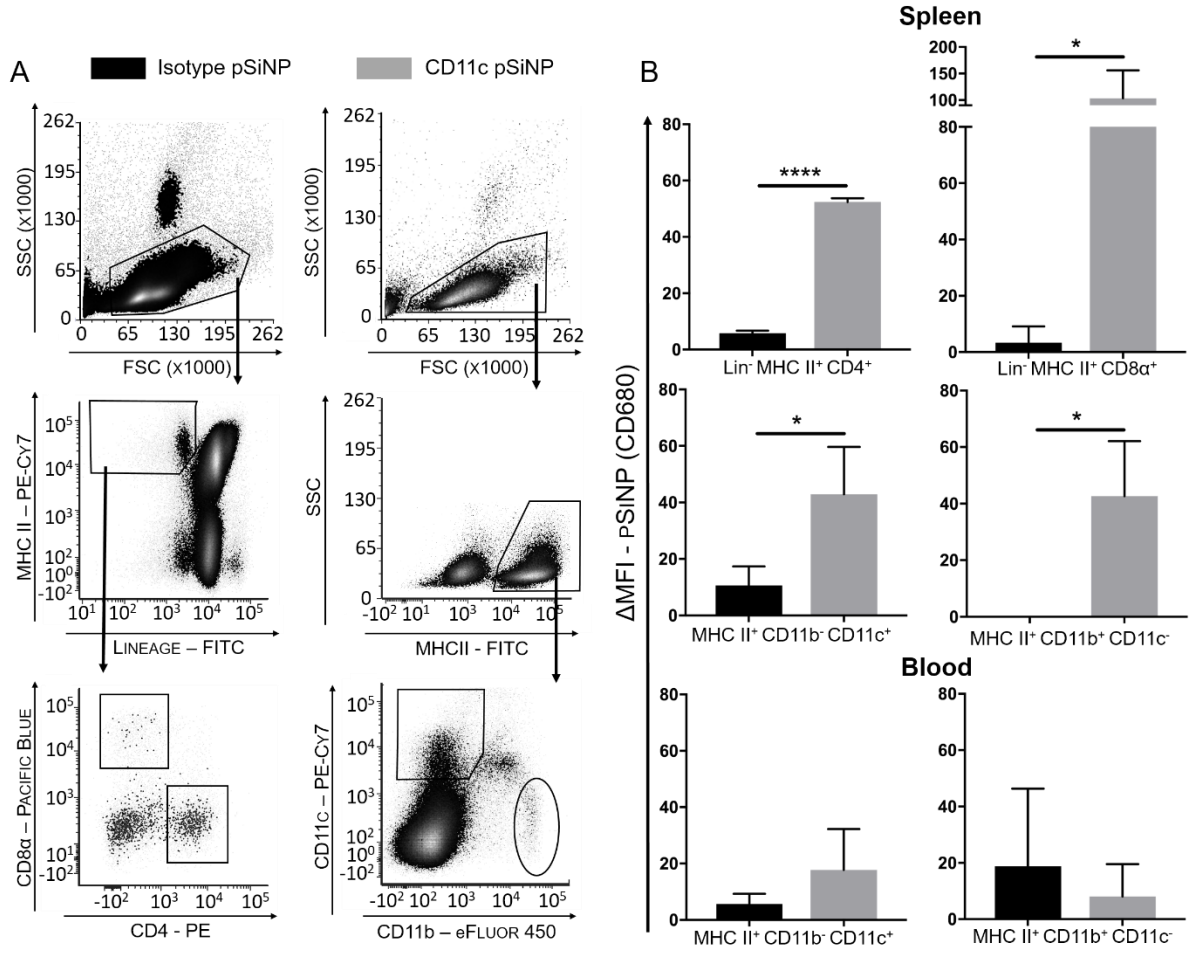


Figure 2. **CD11c pSiNP track to murine splenic myeloid CD4$^+$ and CD8α$^+$ DC *in vivo*.** (A) Gating strategy of lineage negative MHC II$^+$ CD4$^+$ or CD8α $^+$ DC, MHC II$^+$ CD11b$^-$CD11c$^+$ DC and MHC II$^+$ CD11b$^+$ CD11c$^-$ macrophages. (B) Quantification of the mean fluorescence intensity (MFI), representative of pSiNP accumulation, within splenic and blood DC and macrophage populations. CD4$^+$ and CD8α$^+$ DC showed an approximate 9-fold and 31-fold higher levels of CD11c pSiNP respectively in the spleen at 24 h. Data are presented as delta (Δ) MFI ± SD, normalised to the baseline fluorescence levels in saline injected control animals. (n = 3 per group, statistical significance determined by two-tailed T-test, * $p < 0.05$, **** $p < 0.0001$).

Histological sections displayed brown aggregates in the liver and spleen of CD11c-pSiNP and isotype-pSiNP mice respectively (Figure S3). No large aggregates were observed in the heart, lungs or kidneys. The organs appeared healthy compared to the control animals, with no detectable

inflammation. CD11c (PE) and MHC II (FITC) splenic staining confirmed co-localisation of CD11c and pSiNP supporting observations from flow cytometry (Figure S3).

Murine Regulatory T-cell Generation with pSiNP

The pSiNP pores (21 ± 11 nm diameter), allow them to be loaded with drugs and peptides.[17] We recently showed consistent rapamycin loading (5% w/w), via passive diffusion into the pSiNP pores. This loading regime equated to 1 mg/kg of rapamycin per 20 mg/kg of pSiNP.[13] $CD4^+CD25^+FoxP3^+$ splenic Treg concentration in CD11c-pSiNP (rapamycin + $OVA_{323-339}$) OVA sensitised mice was 5-fold higher ($p < 0.01$), 40 days following final intravenous injection, compared to saline control, positive control, fRapamycin, (± $fOVA_{323-339}$) and isotype-pSiNP (OVA + rapamycin) mice (Figure 3).

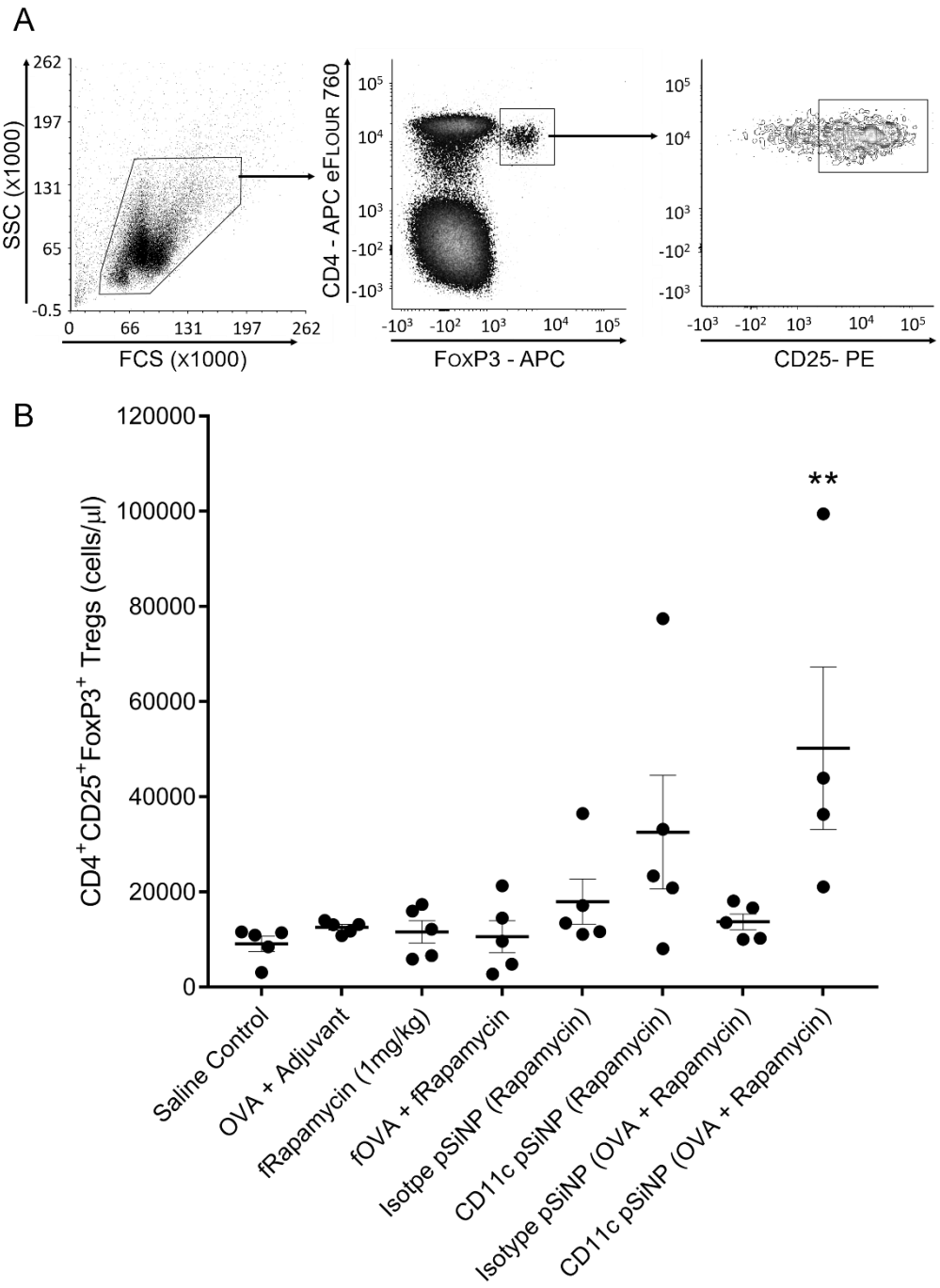


Figure 3. Injections of rapamycin and peptide loaded CD11c pSiNP promote Treg production *in vivo* up to 40 days post injection. (A) Gating strategy of murine splenic $CD4^+FoxP3^+CD25^+$ Treg. (B) Treg were counted using flow cytometer counting beads to determine the concentration of Treg in ovalbumin sensitised mice spleen. Mice which received CD11c pSiNP (i.v.) loaded with $OVA_{323-339}$ peptide and rapamycin showed an approximate 5-fold increase in the number of splenic Treg compared to the untreated

control mice and mice receiving free rapamycin and/or peptide (fRapamycin ± fOVA) with or without pSiNP delivery. (Data are represented as mean ± SEM, n = 5 per group with the exception of CD11c pSiNP (OVA + Rapamycin) n = 4, statistical significance determined by one-way ANOVA, ** $p < 0.01$).

Non-human primate DC targeting DC-SIGN-pSiNP

DC specific receptor DC-SIGN is expressed on non-human primate and human DC.[18] Isotype and DC-SIGN-pSiNP accumulated predominantly in the kidneys and liver, with DC-SIGN-pSiNP also showing up in the lungs of the marmosets (Figure 4). Isotype-pSiNP marmoset organs displayed high kidneys ($3.0x10^8$ RE), liver ($1.8x10^8$ RE) and spleen ($1.4x10^8$ RE) fluorescence, with small amounts detected in the lungs ($2.5x10^7$ RE) and heart ($2.5x10^7$ RE). DC-SIGN-pSiNP tracked mostly to the kidneys ($5.0x10^8$ RE), followed by the liver ($6.5x10^7$ RE), lungs ($5.0x10^7$ RE), heart ($3.9x10^7$ RE), and spleen ($1.0x10^7$ RE) within 24 h.

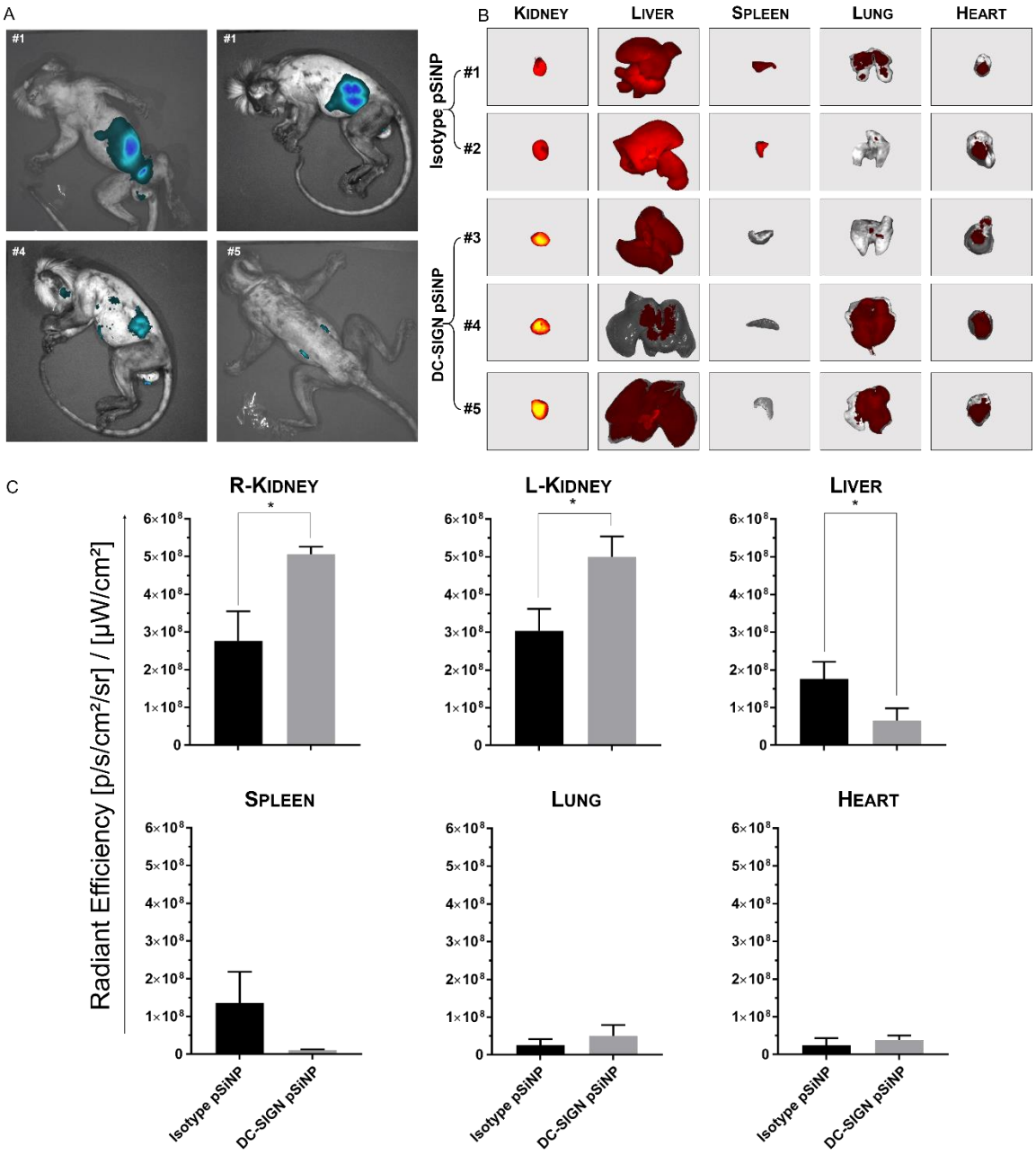


Figure 4. CD-SIGN pSiNP track predominately to the kidneys, followed by the liver, spleen, lungs and heart. (A) Topographical distribution of fluorescent pSiNP in marmosets at 24 h indicated by blue colour. Isotype pSiNP (top) accumulated around kidneys and liver; DC-SIGN pSiNP (bottom), present in the kidneys and lungs of marmosets. (B) Individual organs taken from the marmosets at 24 h post injection (i.v.) with fluorescent pSiNP. Heat map (red to yellow) indicates presence of pSiNP. (C) Quantification of total fluorescence as radiant efficiencies of each of the organs at 24 h. Marmosets injected with CD11c pSiNP showed a higher levels in the kidneys compared to marmosets which received isotype pSiNP. DC-SIGN pSiNP tracked highly to the lungs of the animals. DC-SIGN pSiNP has significantly greater deposition within the kidneys compared to isotype pSiNP, which were seen to accumulate significantly more within the livers of the marmosets. (Data are represented as mean ± SD, isotype pSiNP n = 2, DC-SIGN pSiNP n = 3, significance determined by two-tailed T-test, * $p < 0.05$).

The lineage negative, MHC II^+CD11c^+ splenic myeloid DC population indicated a 3.5-fold uptake increase of the isotype-pSiNP compared to the DC-SIGN-pSiNP. Blood myeloid DC had detectable levels of DC-SIGN-pSiNP in one third of the marmosets whereas isotype-pSiNP were not seen in blood myeloid DC (Figure 5). Splenic $CD14^+$ monocytes showed an uptake of DC-SIGN-pSiNP with no detectable levels of isotype-pSiNP. Blood monocytes accumulated isotype-pSiNP approximately 2-fold more than DC-SIGN-pSiNP, although no significant difference was observed (Figure 5). Splenic $CD20^+$ B-cells showed a 7-fold greater positivity for isotype-pSiNP compared to DC-SIGN-pSiNP. No off-targeting uptake of pSiNP was observed by $CD3^+$ T-cells and $CD56^+$ natural killer cells.

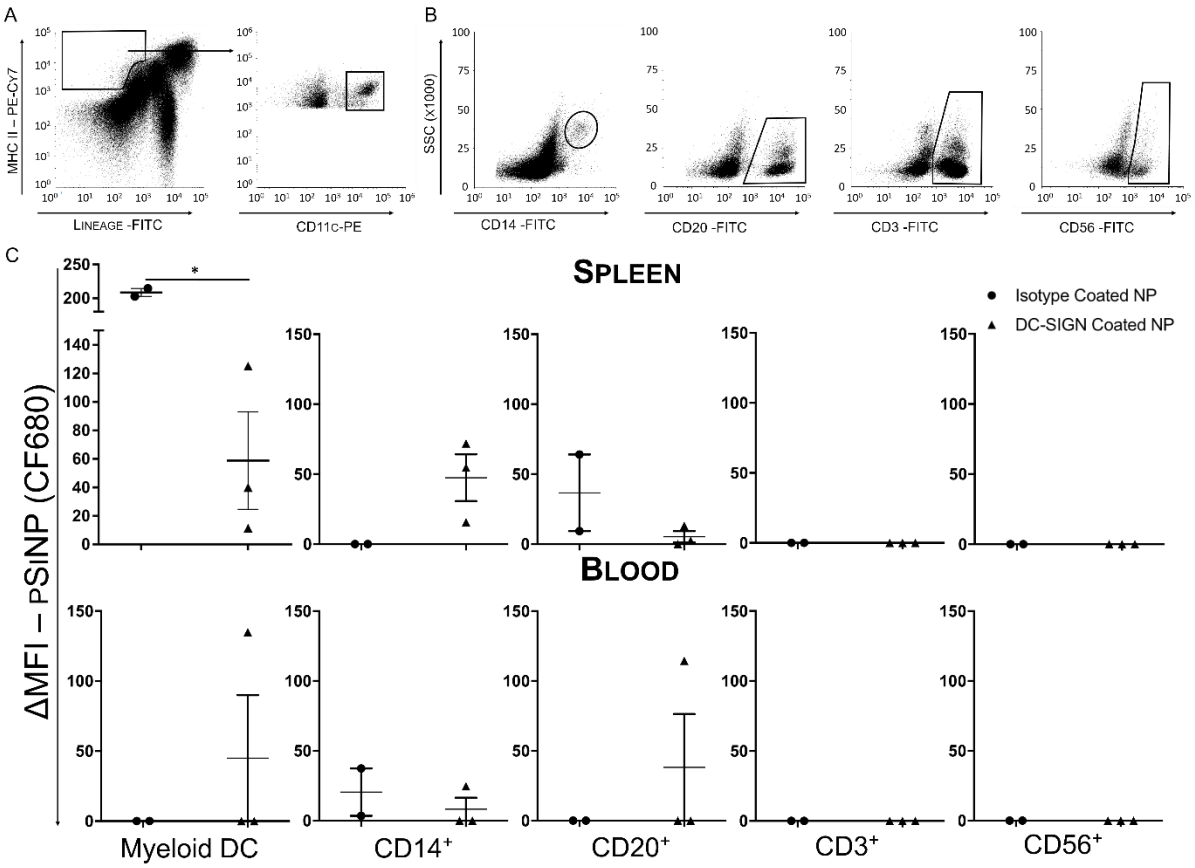


Figure 5. Flow cytometric of marmoset cellular uptake of pSiNP. (A) Marmoset gating strategy of lineage negative MHC II^+ $CD11c^+$ myeloid DC. (B) Gating of monocytes (CD14), B-cells (CD20), T-cells (CD3) and natural killer cell (CD56) populations for flow cytometry. (C) Splenic and peripheral blood cell populations nanoparticle uptake. A higher proportion of isotype pSiNP were phagocytosed by splenic myeloid DC compared to DC-SIGN pSiNP. (Data are presented as ΔMFI ± SEM. Isotype pSiNP n = 2, DC-SIGN pSiNP n = 3, statistical significance determined by two-tailed T-test, * $p < 0.05$)

Urine analysed by inductive-coupled plasma mass spectrometry (ICP-MS) quantified boron and silicon deposits within the urine. Isotype-pSiNP marmosets displayed a 10-fold (6 ppm) and 7-fold (103 ppm) higher concentration of boron and silicon in the urine respectively, compared to DC-SIGN-pSiNP marmosets (Figure 6).

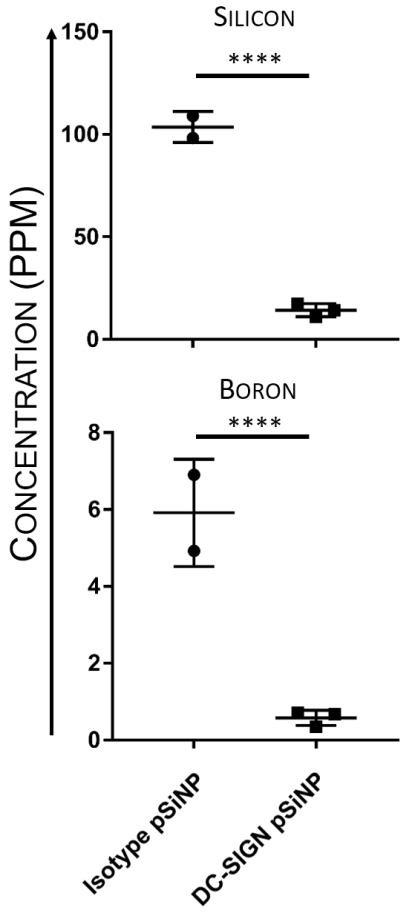


Figure 6. Isotype pSiNP are secreted more readily then DC-SIGN pSiNP in NHP. The porous silicon nanoparticles injected into the marmosets were produced from wafers doped with boron to produce optimal resistivity for pSiNP etching. Due to this process, silicon and boron are the two major degradation products of the pSiNP and can hence be used to measure particle secretion. Marmosets injected with DC-SIGN pSiNP had an approximately 7-fold and 10-fold lower concentration of silicon and boron in their urine, respectively. (Data are representative of mean ± SD, n = 2 (isotype pSiNP) n = 3 (DC-SIGN pSINP). Statistical significance was determined by two-tailed T-test, **** $p < 0.0001$).

pSiNP were detected within the liver, heart, lungs and kidneys of the marmosets, with few detectable clusters present in the spleen (Figure S4). DC-SIGN-pSiNP marmoset lungs showed aggregates ranging from 1 - 10 μm in size and were more dispersed throughout the tissue compared to the isotype-pSiNP marmosets (≤ 8 μm). Ten micrometre clusters in livers from pSiNP DC-SIGN-pSiNP marmoset could be seen, with isotype-pSiNP marmoset clusters generally smaller (≤ 4.5 μm).

Discussion

This study utilised DC-targeted-pSiNP functionalised with anti-CD11c or anti-DC-SIGN antibodies to investigate biodistribution *in vivo*. DC are the most potent of the APC, responsible for phagocytosis and presentation of foreign peptides and maintenance of immunological self-tolerance. A lack of co-stimulatory marker expression by tol-DC promotes T-cell anergy and induces $FoxP3^+$ regulatory T-cells.[11] As DC are key immune cells, there is significant benefit to targeting them *in vivo* to treat cancer, induce tolerance and develop new vaccines. Wierecky *et al.* utilised HLA-A2-binding MUC1 peptide pulsed autologous mature DC, subcutaneously injected into patients with renal cell carcinoma, successfully demonstrating tumour regression.[19] Intravenous delivery of *ex vivo* modified tol-DC, has also prolong allogeneic kidney graft survival in NHP.[20] These methods utilised *ex vivo* modification of DC prior to infusion. The emerging field of nanomedicine can bypass this modification by their targeted therapeutic delivery mechanisms.[21] We successfully targeted DC populations within murine and NHP animal models. Ovalbumin sensitised mice demonstrated a significant 5-fold increase in Tregs, maintained for up to 40 days post-injections. We have established an alternative method of drug delivery to induce Treg

generation completely *in vivo* whilst reducing off-targeting effects shown by enhanced delivery with DC-targeting antigens functionalised pSiNP.

Neither mice nor NHP showed adverse reaction to intravenous administration of pSiNP. DC-targeting pSiNP in both models showed systemic distribution to the kidneys, liver, spleen and lungs. Large nanoparticles (≈ 200 nm) have been shown to aggregate *in vivo* by activating the intrinsic coagulation system.[22] Clot formation promotes fibrinogen and globulin binding to nanoparticle surface, known as corona formation.[23] These proteins unfold, linking to adjacent nanoparticles causing aggregates.[24] Furthermore, nanoparticle induced unfolding of fibrinogen, promotes macrophage activation by Mac-1 (CD11b) binding.[25] Intravenous pSiNP administration in mice travelled via the vena cava to the heart. Large pSiNP aggregates would travel unencumbered through larger atrial and ventricular spaces, resulting in minimal accumulation, which was consistent in both animal models and evident from the low organ fluorescence (figure 1 & 4). The pulmonary circulation offers a site of restricted movement, due to alveolar capillaries, providing an optimal location for pSiNP aggregation, indicative of increase lung fluorescence. This accumulation may be enhanced by the presence of pulmonary macrophages.[26] Arterial circulation carries pSiNP to the liver, spleen, and kidneys. pSiNP uptake in the liver could be attributed to the non-specific phagocytic nature of liver Kupffer cells,[27] one of the most abundant populations of macrophages, resulting in the increased fluorescence (Figure 1). We observed CD11c-pSiNP preferentially tracked to the spleen compared to isotype-pSiNP as well as accumulated significantly in the kidneys compared to all other organs. These pSiNP degrade by 90% within 24 h.[13] Once broken down, covalent linkages between the fluorescent dye and nanoparticles are severed, resulting in renal excretion.[28]

The NHP circulation is identical to mice, with the femoral vein travelling to the inferior vena cava via the iliac vein. However, distribution of pSiNP was markedly different. Marmosets displayed high levels of pSiNP accumulation within the lungs. This phenomenon was augmented in marmosets injected with DC-SIGN-pSiNP, potentially reducing the levels of DC-SIGN-pSiNP in the liver compared to the isotype-pSiNP (Figure 4). The undiagnosed, histologically indicative, chronic lung disease in the marmosets (average age 13 years) compared to juvenile (6-8 weeks) mice, may explain this finding. Splenic deposition was also different compared to the mice. Isotype-pSiNP accumulated in the spleen more than the DC-SIGN-pSiNP. In accordance with the murine model, kidney fluorescence intensity was significantly higher in DC-targeting-pSiNP marmosets. Urine analysis showed that although marmosets had a larger accumulation of DC-SIGN-pSiNP within the kidneys, isotype-pSiNP marmosets secreted 7-fold higher silicon concentrations, suggesting prolonged DC-SIGN-pSiNP retention.

Cytometric analysis of murine and marmoset splenic DC subsets reflected the total splenic fluorescence. CD11c-pSiNP mice had significantly greater fluorescence within the spleens and significantly higher uptake by lineage negative, MHC $CII^{+}CD4^{+}$ and $CD8\alpha^{+}$ conventional DC populations. $CD4^{+}$ and $CD8\alpha^{+}$ DC had 9-fold and 31-fold higher fluorescence intensities in CD11c-pSiNP mice respectively, highlighting the importance of nanoparticle functionalisation with antibodies to preferentially target some of the least abundant cells. A higher concentration of CD11c-pSiNP in the spleen increases the chance of non-specific uptake, indicated by CD11c-pSiNP fluorescence in $CD11b^{+}CD11b^{-}$ macrophages (Figure 2). The uptake of pSiNP within $CD11c^{+}$ blood DC was significantly reduced compared to the spleen with little fluorescence observed. Blood $CD11b^{+}$ macrophages were more positive for isotype-pSiNP compared to CD11c-pSiNP, potentially due to the increased targeting and uptake of CD11c-pSiNP by DC resulting in

fewer circulating CD11c-pSiNP remaining for macrophage phagocytosis. Confocal microscopy of the spleen showed that CD11c-pSiNP were more abundant and highly distributed throughout, compared to isotype-pSiNP (Figure S2).

pSiNP tracking to marmoset splenic myeloid DC produced contrary results. Isotype-pSiNP were phagocytosed 3.5-fold more by the lineage negative, MHC $CII^{+}CD11c^{+}$ myeloid DC, whilst DC-SIGN-pSiNP were taken up predominately by $CD14^{+}$ monocytes. One DC-SIGN-pSiNP marmoset showed a high level of pSiNP uptake by blood $CD11c^{+}$ DC. This particular marmoset also displayed minimal fluorescence in the lungs compared to the other two injected with DC-SIGN-pSiNP. Since pSiNP were not trapped within the pulmonary circulation in that marmoset, they could remain in the circulation until they reached the spleen. The remaining two DC-SIGN-pSiNP marmosets had significantly higher lung accumulation of pSiNP, which would decrease circulating mass. Primate histology revealed chronic lung damage and inflammation, best characterised as chronic airways disease, potentially due to their age. The pathology seen in the lung may have promoted alveolar macrophage recruitment[29, 30] resulting in a higher degree of non-specific phagocytosis of pSiNP. Alternatively, pulmonary DC within the lungs may have been targeted by the particles.

The different tracking ability of DC-targeting-pSiNP in murine and NHP models may also be explained by the difference in targeting antigens and animal species. These data showed that CD11c-pSiNP promoted DC specific targeting to a greater extent than DC-SIGN-pSiNP. Murine DC-SIGN was not utilised due to its expression on only $CD4^{+}$ conventional DC as well as placmacytoid pre-DC lineages.[31] Therefore, CD11c was more analogous to human DC-SIGN, being expressed on only murine myeloid DC lineages. We have also established the use of this cross-reactive human DC-SIGN antibody clone to classify marmoset monocyte-derived DC.[32]

Tol-DC lack the necessary co-stimulatory markers required for naïve T cell activation. Instead, tol-DC differentiate naïve T-cells into Treg or enhance the function of pre-existing Treg. Upon repeated stimulation with the ovalbumin protein on days 33, 47 and 61, the rapamycin and $OVA_{323-339}$ peptide preconditioned DC would continue to phagocytose and process the OVA protein for continued promotion of the discrete pool of OVA reactive regulatory T-cells. Ovalbumin sensitised CD11c-pSiNP (rapamycin + $OVA_{323-339}$) mice showed a significantly (5-fold) higher level of Treg compared to the mice treated with i.v. rapamycin or isotype-pSiNP. This finding demonstrates the importance of nanoparticle functionalisation with cell targeting antibodies. We have expanded on our *in vitro* work where we induced tol-DC with rapamycin loaded pSiNP [13] by promoting Treg expansion completely *in vivo*. Future experiments utilising these pSiNP should explore longer time points to follow Treg fate. We previously demonstrated the ability to produce camptothecin loaded silicon nanoparticles, nanodiscs and silica nanopills for the targeted killing of neuroblastoma cancer cells.[33-35] We have now explored the potential of these pSiNP within a transplant immunology setting. Translation of this protocol into a transplantation model to induce graft tolerance without *ex vivo* DC modification would be highly beneficial in exploring the full extent of these nanoparticles.

Pathological changes, potentially due to age related illness, may have resulted in the high pSiNP tracking variability within the DC-SIGN-pSiNP animal test group, potentially skewing the *in vivo* tracking abilities and is a main limitation within this study. The lack of a completely identical targeting antigen between the murine and NHP animal models also made it difficult to compare pSiNP uptake between the two species. Potential future directions include functionalising pSiNP with marmoset reactive CD11c antibody, identifying if this promotes DC uptake within the spleen. Younger marmosets should also be utilised for these experiments, as it was seen that one of the

DC-SIGN-pSiNP marmosets did display tracking abilities to both splenic and blood DC *in vivo* suggesting a potentially highly beneficial method for targeting both populations of DC.

Conclusion

In conclusion, pSiNP displaying DC-targeting mAb were well tolerated in mice and in NHP. The animals showed no adverse side effects or embolism from particle aggregation. Effective targeting to blood and tissue DC was demonstrated. pSiNP loaded with rapamycin targeting CD11c promoted the generation of Treg *in vivo* without the more commonly used preliminary *ex vivo* modification of DC. An unexpected and interesting finding was the enhanced kidney targeting ability of DC-targeting pSiNP, demonstrating a significantly higher renal tracking capability in murine and NHP models, compared to isotype-pSiNP. Taking in conjunction with our recent findings that pSiNP can modify DC function *in vitro*, this study provides further *in vivo* validation for the potential of targeted nanomedicine for future drug delivery in transplantation and other immune mediated diseases.

Materials and Methods

Mice

Male C57BL/6 mice 7-8 weeks old were purchased from Animal Resources Centre, Western Australia. Mice received intravenous (i.v.) injections of pSiNP (20 mg/kg) coated with purified Armenian hamster isotype control monoclonal antibody (mAb) (BD Biosciences, California, USA. Clone G94-56) or purified Hamster anti-mouse CD11c mAb (BD Biosciences. Clone HL3). Animals were imaged at 1, 6, 12 and 24 h. Mice were maintained in the University of Adelaide

Animal Facility in accordance with Australian animal ethics guidelines, application 20123 and 31951.

Marmosets

Common Marmoset (*Callithrix jacchus*) monkeys were housed at The Queen Elizabeth Hospital Animal house. Marmosets received i.v. injections via left femoral vein, of pSiNP (20 mg/kg) coated in purified isotype control (eBioscience, California, USA, Clone eBMG2b) or DC-SIGN mAb (BD Biosciences, Clone DCN46). Animals were euthanised 24 h post injection. Prior to the autopsy, marmosets were imaged to obtain a topographic distribution of pSiNP. Marmosets were maintained at the Queen Elizabeth Hospital Animal Facility in accordance with the NHMRC Australian guidelines for the holding and use of non-human primates for medical research. CALHN animal ethics committee approval number 55-15.

Immunisation Protocol

C57BL/6 mice immunisation protocol was adapted from Maldonado *et al.*[12] Mice were subcutaneously injected with 100 µg of ovalbumin protein (Grade V, Sigma. Missouri, USA) admixed 1:1 (v/v) in saline and Alhydrogel® adjuvant (InvivoGen, California, USA), to a final volume of 100 µl on days 0, 14 and 28. Concurrently, mice received a 100 µl i.v. injection of saline, free rapamycin (fRapamycin, 1 mg/kg), 100 µg fluorescently labelled free $OVA_{323-339}$ peptide (FITC-βAla-ISQAVHAAHAEINEAGR-OH, Auspep, Victoria, Australia) (fOVA) and fRapamycin, or isotype or CD11c-pSiNP loaded with rapamycin and/or $OVA_{323-339}$. Challenges of

100 µg of OVA protein were given on days 33, 47 and 61 subcutaneously. Mice were humanely euthanised on day 68.

Preparation of pSiNP

pSiNP were prepared as previously described.[13] Silicon wafers were electrochemically etched and polished in aqueous hydrofluoric acid. The porous layer was fractured by ultrasonication and filtered. Filtrate was resuspended in a 0.1 M solution of protected semicarbazide (tert-butyl-2-[(allylamino)carbonyl] hydrazine-carboxylate)[14] in tetrahydrofuran for 3 h at 85 ˚C under N_2 reflux. Nanoparticles were rinsed twice in tetrahydrofuran and twice in ethanol (EtOH) and stored at 4 ˚C.

Drug and Peptide Loading of pSiNP

Boc-group was removed from the protected semicarbazide by resuspending pSiNP in a 2:3 solution of dichloromethane and trifluoroacetic acid and agitated (4 h, room temperature (RT)) and washed once in dichloromethane, twice in EtOH and twice in saline (22,000g, 10 min).[13] pSiNP were loaded with rapamycin, with or without fluorescently labelled $OVA_{323-339}$ peptide. Deprotected pSiNP were resuspended in a solution of rapamycin dissolved in EtOH (2 mg/ml) and incubated for 2 h at RT. The pSiNP were washed once in saline and resuspended in a solution of $OVA_{323-339}$ (1:5 ratio of peptide to pSiNP) in saline (10 min, RT) before the addition of the oxidised antibody.

Antibody and Fluorophore Coating of pSiNP

Antibody attachment to pSiNP was as previously described.[13] Antibodies and appropriate isotype matched controls were admixed with of sodium periodate and placed on an orbital shaker in the dark for 30 min (RT, 60 rpm). Antibodies were washed in PBS with centrifugal concentrators (Sartorius, Germany). Nanoparticles were resuspended in oxidised antibody for 30 min and agitated. Antibody binding was confirmed by measuring the UV absorbance (280 nm) (Nanodrop 2000, Thermo Scientific, Massachusetts, USA). For the tracking experiments, antibody-labelled pSiNP were pelleted and resuspended in a solution of XenoLight CF680 succinimidyl ester (SE) dye (Perkin Elmer. Massachusetts, USA) dissolved in a 1 mM solution of sodium carbonate buffer (pH = 9). Samples were placed in the dark on an orbital shaker for 1 h (RT, 60 rpm). Nanoparticles were washed several times in saline (22,000 x g, 2 min) until the supernatant was colourless and resuspended in saline and sonicated thoroughly immediately prior to injection.

In Vivo and Ex Vivo Fluorescence Imaging

Animals or their kidneys, livers, hearts, lungs and spleens were placed in an IVIS Lumina Series III Imaging System (Caliper Life Sciences, Massacutests, USA). The charge-coupled device camera obtained fluorescence images utilising the appropriate filter combinations (excitation 660 nm, emission 680-700 nm). Reflected light photographs were overlayed with fluorescent images and analysed using Living Images 4.5.5 software. Signal intensity was assessed by radiant efficiencies (RE) ([p/s/cm^2/sr]/[μW/cm^2]).

Murine and Non-Human Primate Splenocyte Processing

Harvested spleens were kept at 4 °C in RPMI 1640 (Invitrogen, Massachusetts, USA). Spleens were homogenised through a 70 μm filter and resuspended in 50 ml in PBS. Filtrate was centrifuged, 450 x g for 7 min at room temperature (RT). The supernatant was discarded and the pellet resuspended in 10-30 ml of red blood cell lysis buffer (155 mM NH_4Cl, 5 mM $NaHCO_3$, 127 μM EDTA) and incubated at 37 °C for 10 min. Cells were washed in PBS (1% heat inactivated Foetal Calf Serum (FCS)). Splenocytes were resuspended in FACS wash buffer (phosphate buffered saline (PBS), 1% FCS, 20 mM sodium azide) containing 10% heat inactivated rabbit serum to a concentration of $1x10^6$ cell/ml and blocked for 20 min (RT) before flow cytometry staining.

In vivo Tracking Flow Cytometry Staining

Whole blood or splenocytes were stained with antibodies (table S1 & S2) and incubated at 4 °C for 30 min. After incubation, FACS lysing solution (BD Biosciences) was added to the splenocytes and the whole blood, 1 ml or 2 ml, respectively and vortexed. The cells were washed in wash buffer until supernatants were clear and resuspended in 200 μl wash buffer before acquisition on a FACSCanto II (BD Biosciences) and analysis with FCS Express v6 (De Novo Software, Glendale, CA).

Regulatory T-cell Staining

Murine splenic Treg were stained as per manufacturer's instructions (Treg detection kit, Miltenyi Biotec. Bergisch Gladbach, Germany). Briefly, $2x10^6$ splenocytes were resuspended in 100 µl of wash buffer with the addition of CD4 (clone GK1.5, eBioscience) and CD25 (clone 7D4, Miltenyi Biotec) antibodies. The cells were incubated in the dark (10 min, 4˚C). Splenocytes were washed in wash buffer (300 x g for 5 min) and resuspended in fix/perm buffer (30 min, 4 ˚C). Splenocytes were washed in wash buffer and permeabilisation buffer before the addition of FoxP3 antibody (30 min, 4˚C). Prior to acquisition on a FACSCanto II, APC Calibrite™ counting beads (BD Biosciences) were added.

Scanning Electron Microscopy (SEM)

Tissue sections were gradient dehydrated (70% - 90% 10 min, RT) and 100% (2x, 10 min, RT) in undenatured EtOH devoid of silicon. Samples were allowed to air dry and placed on an aluminium SEM mounting stub (Ted Pella, California, USA) and splutter coated (Quorum Q150T ES, Quorum Technologies. Lewes, UK) with carbon. Samples were imaged with a XL30 SEM (Philips Electrical Company, Amsterdam, Netherlands)

Histopathological analyses

Organs were fixed in 10% formaldehyde for light microscopic examination. Following routine dehydration and transparency procedures, the tissues were embedded in paraffin blocks. Five

micrometre sections were melted onto Superfrost microscope slides (Thermo Scientific). Sections were stained with hematoxylin and eosin (H&E).

Immunofluorescence

Optimal cutting temperature (OCT) compound (Agar Scientific. Essex, United Kingdom) embedded murine tissues were sectioned and transferred to slides. Unfixed tissues were stained via direct immunofluorescence. Sections were equilibrated to RT and washed in PBS for 5 min. Sections were then incubated at RT for 30 min in 10% blocking buffer before primary conjugated antibody was added for 1 h, in the dark. Sections were washed in PBS (2 x 5 min) before the addition of DAPI (4', 6'-diamidino-2-phenylindole) (Biolegend. California, USA) for nucleus staining and mounting with fluorescent mounting media (Dako, Glostrup Municipality, Denmark)

Inductively-Coupled Plasma Mass Spectrometry (ICP-MS)

Urine samples taken from the marmosets were diluted in ICP-MS buffer (2% 1-butanol, 0.05% EDTA, 0.05% Triton X-100 and 1% NH_4OH in water) and run on an Agilent 8800 Triple Quadrupole ICP-MS (Agilent Technologies, California, USA).

Acknowledgements

We would like to acknowledge Ms. M. Archer and Ms. L. Hodson for their assistance with tissue processing. Mr. M. Smith, facility manager of the Queen Elizabeth Hospital animal house and Dr. D. Noonan and Dr. T. Kuchel for their assistance with animal procedures. We would also like to acknowledge the University of Adelaide, Adelaide Microscopy (AM) and the Australian Microscopy Microanalysis Research Facility (AMMRF).

This work was performed in part at the Melbourne Centre for Nanofabrication (MCN) in the Victorian Node of the Australian National Fabrication Facility (ANFF).

Supporting Information Available:

This material is available free of charge via the internet at http://pubs.acs.org.

References

1. Chatrath H, Berman K, Vuppalanchi R, Slaven J, Kwo P, Tector AJ, et al. De novo malignancy post–liver transplantation: a single center, population controlled study. Clinical transplantation. 2013;27(4):582-90.

2. Tilney NL. Transplant: from myth to reality: Yale University Press; 2003.

3. Maldonado RA, von Andrian UH. How tolerogenic dendritic cells induce regulatory T cells. Advances in immunology. 2010;108:111.

4. Coates PTH, Thomson AW. Dendritic cells, tolerance induction and transplant outcome. American Journal of Transplantation. 2002;2(4):299-307.

5. Coates PTH, Barratt-Boyes SM, Donnenberg AD, Morelli AE, Murphey-Corb M, Thomson AW. Strategies for preclinical evaluation of dendritic cell subsets for promotion of transplant tolerance in the nonhuman primate. Human immunology. 2002;63(10):955-65.

6. Thomson AW, Zahorchak AF, Ezzelarab MB, Butterfield LH, Lakkis FG, Metes DM. Prospective clinical testing of regulatory dendritic cells in organ transplantation. Frontiers in immunology. 2016;7.

7. Sehgal SN. Rapamune®(RAPA, rapamycin, sirolimus): mechanism of action immunosuppressive effect results from blockade of signal transduction and inhibition of cell cycle progression. Clinical biochemistry. 1998;31(5):335-40.

8. Silk KM, Leishman AJ, Nishimoto KP, Reddy A, Fairchild PJ. Rapamycin conditioning of dendritic cells differentiated from human ES cells promotes a tolerogenic phenotype. BioMed Research International. 2012;2012.

9. Taner T, Hackstein H, Wang Z, Morelli AE, Thomson AW. Rapamycin-Treated, Alloantigen-Pulsed Host Dendritic Cells Induce Ag-Specific T Cell Regulation and Prolong Graft Survival. American Journal of Transplantation. 2005;5(2):228-36.

10. Turnquist HR, Raimondi G, Zahorchak AF, Fischer RT, Wang Z, Thomson AW. Rapamycin-conditioned dendritic cells are poor stimulators of allogeneic CD4+ T cells, but enrich for antigen-specific Foxp3+ T regulatory cells and promote organ transplant tolerance. The Journal of Immunology. 2007;178(11):7018-31.

11. Pothoven K, Kheradmand T, Yang Q, Houlihan J, Zhang H, Degutes M, et al. Rapamycin-Conditioned Donor Dendritic Cells Differentiate CD4+ CD25+ Foxp3+ T Cells In Vitro with TGF-β1 for Islet Transplantation. American Journal of Transplantation. 2010;10(8):1774-84.

12. Maldonado RA, LaMothe RA, Ferrari JD, Zhang AH, Rossi RJ, Kolte PN, et al. Polymeric synthetic nanoparticles for the induction of antigen-specific immunological tolerance. Proceedings of the National Academy of Sciences of the United States of America. 2015;112(2):E156-65.

13. Stead SO, McInnes SJ, Kireta S, Rose PD, Jesudason S, Rojas-Canales D, et al. Manipulating human dendritic cell phenotype and function with targeted porous silicon nanoparticles. Biomaterials. 2017.

14. Coffinier Y, Olivier C, Perzyna A, Grandidier B, Wallart X, Durand JO, et al. Semicarbazide-functionalized Si(111) surfaces for the site-specific immobilization of peptides. Langmuir. 2005;21(4):1489-96.

15. Edwards AD, Chaussabel D, Tomlinson S, Schulz O, Sher A, e Sousa CR. Relationships among murine CD11chigh dendritic cell subsets as revealed by baseline gene expression patterns. The Journal of Immunology. 2003;171(1):47-60.

16. Gonçalves R, Mosser DM. The isolation and characterization of murine macrophages. Current protocols in immunology. 2015:14.1. 1-.1. 6.

17. Cifuentes-Rius A, Ivask A, Sporleder E, Kaur I, Assan Y, Rao S, et al. Dual-Action Cancer Therapy with Targeted Porous Silicon Nanovectors. Small. 2017.

18. Jesudason S, Collins MG, Rogers NM, Kireta S, Coates PTH. Non-human primate dendritic cells. Journal of leukocyte biology. 2012;91(2):217-28.

19. Wierecky J, Müller MR, Wirths S, Halder-Oehler E, Dörfel D, Schmidt SM, et al. Immunologic and clinical responses after vaccinations with peptide-pulsed dendritic cells in metastatic renal cancer patients. Cancer Research. 2006;66(11):5910-8.

20. Ezzelarab M, Zahorchak A, Lu L, Morelli A, Chalasani G, Demetris A, et al. Regulatory dendritic cell infusion prolongs kidney allograft survival in nonhuman primates. American Journal of Transplantation. 2013;13(8):1989-2005.

21. Fan Y, Moon JJ. Nanoparticle drug delivery systems designed to improve cancer vaccines and immunotherapy. Vaccines. 2015;3(3):662-85.

22. Ilinskaya AN, Dobrovolskaia MA. Nanoparticles and the blood coagulation system. Part II: safety concerns. Nanomedicine. 2013;8(6):969-81.

23. Ajdari N, Vyas C, Bogan SL, Lwaleed BA, Cousins BG. Gold nanoparticle interactions in human blood: a model evaluation. Nanomedicine: Nanotechnology, Biology and Medicine. 2017;13(4):1531-42.

24. Dominguez-Medina S, Kisley L, Tauzin LJ, Hoggard A, Shuang B, DS Indrasekara AS, et al. Adsorption and unfolding of a single protein triggers nanoparticle aggregation. ACS nano. 2016;10(2):2103-12.

25. Deng ZJ, Liang M, Monteiro M, Toth I, Minchin RF. Nanoparticle-induced unfolding of fibrinogen promotes Mac-1 receptor activation and inflammation. Nature nanotechnology. 2011;6(1):39-44.

26. van Oud Alblas AB, Van Furth R. Origin, Kinetics, and characteristics of pulmonary macrophages in the normal steady state. Journal of Experimental Medicine. 1979;149(6):1504-18.

27. Kawada N, Parola M. Interactions of Stellate Cells with Other Non-Parenchymal Cells. Stellate Cells in Health and Disease. 2015:185.

28. Reffitt DM, Jugdaohsingh R, Thompson RP, Powell JJ. Silicic acid: its gastrointestinal uptake and urinary excretion in man and effects on aluminium excretion. Journal of inorganic biochemistry. 1999;76(2):141-7.

29. de BOER WI, van SCHADEWIJK A, Sont JK, Sharma HS, Stolk J, Hiemstra PS, et al. Transforming growth factor β1 and recruitment of macrophages and mast cells in airways in chronic obstructive pulmonary disease. American journal of respiratory and critical care medicine. 1998;158(6):1951-7.

30. Woodruff PG, Ellwanger A, Solon M, Cambier CJ, Pinkerton KE, Koth LL. Alveolar macrophage recruitment and activation by chronic second hand smoke exposure in mice. COPD: Journal of Chronic Obstructive Pulmonary Disease. 2009;6(2):86-94.

31. Caminschi I, Corbett AJ, Zahra C, Lahoud M, Lucas KM, Sofi M, et al. Functional comparison of mouse CIRE/mouse DC-SIGN and human DC-SIGN. International immunology. 2006;18(5):741-53.

32. Prasad S, Kireta S, Leedham E, Russ GR, Coates PTH. Propagation and characterisation of dendritic cells from G-CSF mobilised peripheral blood monocytes and stem cells in common marmoset monkeys. Journal of immunological methods. 2010;352(1):59-70.

33. Secret E, Smith K, Dubljevic V, Moore E, Macardle P, Delalat B, et al. Antibody-Functionalized Porous Silicon Nanoparticles for Vectorization of Hydrophobic Drugs. Advanced healthcare materials. 2013;2(5):718-27.

34. Alhmoud H, Delalat B, Elnathan R, Cifuentes-Rius A, Chaix A, Rogers ML, et al. Porous silicon nanodiscs for targeted drug delivery. Advanced Functional Materials. 2015;25(7):1137-45.

35. Alba M, Delalat B, Formentín P, Rogers ML, Marsal LF, Voelcker NH. Silica nanopills for targeted anticancer drug delivery. Small. 2015;11(36):4626-31.